G3, 2025, **15(5)**, jkaf040
https://doi.org/10.1093/g3journal/jkaf040
Advance Access Publication Date: 24 February 2025
Mutant Screen Report

A deficiency screen of the *X* chromosome for Rap1 GTPase dominant interacting genes in *Drosophila* border cell migration

C. Luke Messer,[1,2] Emily Burghardt ,[1] Jocelyn A. McDonald [1,*]

[1]Division of Biology, Kansas State University, Manhattan, KS 66506, USA
[2]Department of Natural Sciences, The University of Virginia's College at Wise, Wise, VA 24293, USA

*Corresponding author: Division of Biology, Kansas State University, 116 Ackert Hall, 1717 Claflin Road, Manhattan, KS 66506, USA. Email: jmcdona@ksu.edu

Collective cell migration is critical to embryonic development, wound healing, and the immune response, but also drives tumor dissemination. Understanding how cell collectives coordinate migration in vivo has been a challenge, with potential therapeutic benefits that range from addressing developmental defects to designing targeted cancer treatments. The small GTPase Rap1 has emerged as a regulator of both embryogenesis and cancer cell migration. How active Rap1 coordinates downstream signaling functions required for coordinated collective migration is poorly understood. *Drosophila* border cells undergo a stereotyped and genetically tractable in vivo migration within the developing egg chamber of the ovary. This group of 6–8 cells migrates through a densely packed tissue microenvironment and serves as an excellent model for collective cell migration during development and disease. Rap1, like all small GTPases, has distinct activity state switches that link extracellular signals to organized cell behaviors. Proper regulation of Rap1 activity is essential for successful border cell migration yet the signaling partners and other downstream effectors are poorly characterized. Using the known requirement for Rap1 in border cell migration, we conducted a dominant suppressor screen for genes whose heterozygous loss modifies the migration defects observed upon constitutively active $Rap1^{V12}$ expression. Here, we identified 7 genomic regions on the *X* chromosome that interact with $Rap1^{V12}$. We mapped three genomic regions to single Rap1-interacting genes, *frizzled 4*, *Ubiquitin-specific protease 16/45*, and *strawberry notch*. Thus, this unbiased screening approach identified multiple new candidate regulators of Rap1 activity with roles in collective border cell migration.

Keywords: *Drosophila;* border cells; collective cell migration; Rap1 GTPase; *frizzled 4*; *Ubiquitin-specific protease 16/45*; *strawberry notch*; FlyBase

Introduction

The small GTPase Rap1 has important roles in tissue morphogenesis and integrity, single-cell and collective cell migration, wound healing, and tumor invasion in cancer (Zhang *et al.* 2017; Chang *et al.* 2018; Jaśkiewicz *et al.* 2018; Sawant *et al.* 2018; Volovetz *et al.* 2020; Kim *et al.* 2022; Messer and McDonald 2023; Perez-Vale *et al.* 2023; Rothenberg *et al.* 2023; Ueda *et al.* 2023). Rap1, like other small GTPases, acts as a molecular switch with discrete "on" and "off" states. GTPase activity is regulated by a combination of GTPase activating proteins (GAPs) that speed up GTP hydrolysis and result in inactive GDP-bound GTPases, and guanine nucleotide exchange factors (GEFs) that promote dissociation of GDP allowing GTP to bind (Raaijmakers and Bos 2009; Cherfils and Zeghouf 2013; Zegers and Friedl 2014). Several key regulators have been identified for Rap1, including the GAP Rapgap1 and the GEF PDZ-GEF/Dizzy (Boettner and Van Aelst 2009; Wang *et al.* 2013; Jaśkiewicz *et al.* 2018; Sawant *et al.* 2018). Other signaling partners downstream of Rap1, including Afadin/Canoe and Rap1-interacting adaptor molecule (RIAM), promote Rap1-dependent cellular processes such as cell polarity and adhesion (Su *et al.* 2015; Bonello *et al.* 2018; Walther *et al.* 2018; Bromberger *et al.* 2021; Hiremath *et al.* 2023; Rothenberg *et al.* 2023). Despite progress in identifying some Rap1-effectors, our understanding of how Rap1 coordinates a diverse set of functions in a wide range of tissues remains limited, with many Rap1 roles unaccounted for by these known effectors.

To address this gap, we performed an unbiased dominant genetic interaction screen to identify downstream targets of Rap1 and other Rap1-interacting genes in a migrating cell collective, the *Drosophila* border cells. Similar approaches in *Drosophila* models of collective migration and morphogenesis have underscored the power of this technique to quickly identify candidate interacting genes that may otherwise be difficult to uncover (McDonald *et al.* 2003; Ward *et al.* 2003; Patch *et al.* 2009; Geisbrecht *et al.* 2013; Hurd *et al.* 2013; Chang *et al.* 2018). Specifically, we took advantage of the established role of Rap1 in regulating border cell migration, a genetically tractable in vivo model of collective cell migration (Chang *et al.* 2018; Sawant *et al.* 2018). Border cells are a group of 6–8 epithelial cells that are specified and recruited as a migratory cohort (cluster) during stages 8–9 of oogenesis. Subsequently, the border cell cluster delaminates from the epithelium, then migrates between germline-derived nurse cells to reach the oocyte boundary by stage 10. The migration of border

Received on 31 December 2024; accepted on 18 February 2025

cells requires integration of guidance cues with Rac1 GTPase activation, which leads to the production of large migratory protrusions at the cluster leading edge (Wang *et al.* 2010; Montell *et al.* 2012; Fernández-Espartero *et al.* 2013; Ramel *et al.* 2013; Saadin and Starz-Gaiano 2016; Scarpa and Mayor 2016; Roberto and Emery 2022). During the process of border cell collective migration, Rap1 promotes actomyosin polarity, helps restrict protrusions to the leading edge, and contributes to proper E-Cadherin enrichment within the cluster (Chang *et al.* 2018; Sawant *et al.* 2018). We know very little, however, about the Rap1-interacting genes that coordinate these critical Rap1-dependent functions.

Notably, similar to the loss of Rap1 function, expression of constitutively active Rap1 ($Rap1^{V12}$) causes severe border cell migration defects (Chang *et al.* 2018; Sawant *et al.* 2018). Thus, the levels of Rap1 are critical for normal collective cell migration. Here, we leveraged this phenotype to conduct an unbiased screen for genes whose heterozygous loss modifies the constitutively active Rap1 phenotype. Using a publicly available collection of *Drosophila* deficiencies that in total remove ~98% of genes on the X chromosome, we identified 7 genomic regions that dominantly suppressed the $Rap1^{V12}$ migration defects. Through further genetic tests, we mapped three of the interacting regions to individual genes. Specifically, we identified *frizzled 4 (fz4)*, *Ubiquitin-specific protease 16/45* (*Usp16-45*), and *strawberry notch* (*sno*) as genes whose heterozygous loss strongly modified the $Rap1^{V12}$-induced border cell migration defects. Furthermore, we found that loss of *Usp16-45* and *sno* on their own also impaired border cell movement. Thus, this screen identified three genes and four additional genetic interacting regions that represent previously uncharacterized Rap1-interacting genes in collective cell migration.

Materials and methods

Drosophila deficiency screen and genetics

The *X* chromosome deficiency kit (DK1) was obtained from the Bloomington *Drosophila* Stock Center (BDSC). Females from balanced X chromosome deficiency lines were crossed to *slbo*-GAL4/CyO; UAS-$Rap1^{V12}$/TM6B, *tub*Gal80 ("*slbo* > $Rap1^{V12}$") males (Fig. 1a). In the case of w^{1118} controls, flies from the *slbo* > $Rap1^{V12}$ stock were crossed to w^{1118}. F1 progeny of the correct genotype (lacking balancer chromosomes) were selected and fattened overnight (~12–24 h) on supplemental yeast at 27°C prior to dissection. Each deficiency in the primary screen was tested at least once; potential interacting deficiency "hits" were then further evaluated. Hits in the primary screen were defined as having at least 50% of border cell clusters migrating more than half of the egg chamber length (the region between the anterior tip and the oocyte anterior border; Fig. 1a). This value is greater than 2 standard deviations above the mean of control egg chambers scored in the primary screen and allowed us to identify high confidence hits. All reported hit lines were subsequently tested a minimum of three times. Potential enhancers were defined as those deficiency regions that resulted in at least 90% of border cell clusters failing to migrate more than half of the egg chamber length. This value is greater than one standard deviation above the mean of control egg chambers. These enhancing deficiencies are flagged in Table 1 but were not pursued further in this study.

To identify relevant genes from the interacting deficiencies, UAS-RNAi lines, and mutant alleles were obtained from the BDSC and the Vienna Drosophila Resource Center (VDRC). For RNAi knockdown of candidate genes, each UAS-RNAi line was crossed to *c306*-GAL4, an early follicle cell driver that has been used for strong RNAi knockdown in border cells (Aranjuez *et al.* 2016; Plutoni *et al.* 2019; Miao *et al.* 2022). To ensure efficient RNAi knockdown, females of the correct genotype were temperature shifted to 29°C for 2 d before being fattened overnight (~12–24 h) on supplemental yeast at 29°C prior to dissection. Similarly, to test interaction with mutant alleles, *slbo*-GAL4/CyO; UAS-$Rap1^{V12}$/TM6b, *tub*Gal80 males were crossed to mutant females, followed by incubation and fattening at 27°C prior to dissection and imaging of migration.

Immunostaining and imaging

Ovaries were dissected in Schneider's *Drosophila* Medium (Thermo Fisher Scientific, Waltham, MA, USA) supplemented with 10% fetal bovine serum (Seradigm FBS; VWR, Radnor, PA, USA). Ovaries were then fixed for 10 mins using 16% methanol-free formaldehyde (Polysciences, Inc., Warrington, PA, USA) diluted to a final concentration of 4% in 1× phosphate-buffered saline (PBS). Following fixation, tissues were washed ≥4x with "NP40 block" [50 mM Tris-HCL, pH 7.4, 150 mM NaCl, 0.5% NP40, 5 mg/ml bovine serum albumin (BSA)] and rocked in the solution for ≥30 mins prior to antibody incubation. Primary antibodies, obtained from the Developmental Studies Hybridoma Bank (DSHB, University of Iowa, Iowa City, IA, USA), were used at the following dilutions: rat anti-E-Cadherin 1:10 (DCAD2) and mouse anti-Singed 1:10–1:25 (Sn7C). For GFP detection, rabbit anti-GFP (A11122, Thermo Fisher Scientific) was used at 1:1,000 dilution. Anti-rat, anti-mouse, or anti-rabbit secondary antibodies conjugated to Alexa Flour-488 or –568 (Thermo Fisher Scientific) were used at 1:400 dilution. 4′, 6′-Diamidino-2-phenylindole (DAPI, Millipore Sigma) was used at 2.5 µg/ml to label nuclei. Primary and secondary antibody incubation as well as all other subsequent wash steps were also performed in NP40 block. Dissected and stained ovarioles and egg chambers were mounted on slides with Aqua-Poly/Mount (Polysciences, Inc.). Images of fixed egg chambers were either acquired on an upright Zeiss AxioImager Z1 microscope with Apotome.2 optical sectioning or on a Zeiss LSM 880 confocal laser scanning microscope (KSU College of Veterinary Medicine Confocal Core) using either a 20× 0.75 numerical aperture (NA) or 40× 1.3 NA oil-immersion objective controlled by Zeiss Zen 14 software. Images were processed in FIJI (Schindelin *et al.* 2012) and figures were assembled using Affinity Photo version 1.10.8 (Serif, Nottingham, United Kingdom). Illustrations were designed in Affinity Photo.

Graphs and statistics

Deficiency regions that were considered "hits" were analyzed for migration a minimum of three times, with a minimum of 20 egg chambers scored per trial. The average of all trials for each "hit" had migration greater than 50% of the migration distance toward the oocyte. This value was determined as >2σ above the mean "migration" for *slbo*-GAL4, UAS-$Rap1^{V12}$/w^{1118} controls under the same conditions. To identify the relevant genes within the deficiency required for border cell migration in the RNAi tests, we defined a migration defect as the fraction of border cell clusters that failed to reach ≥75% of the migration distance to the oocyte. Chi-squared tests were performed to assess the significance level for each experiment using GraphPad Prism 9 (GraphPad Software, San Diego, CA, USA). See Tables 2 and 3 for raw numbers (N's) and statistics. Graphs were assembled in GraphPad Prism 9. Relevant data from the screening approach were included in graphs where appropriate, but statistical testing was limited to experiments with matched controls.

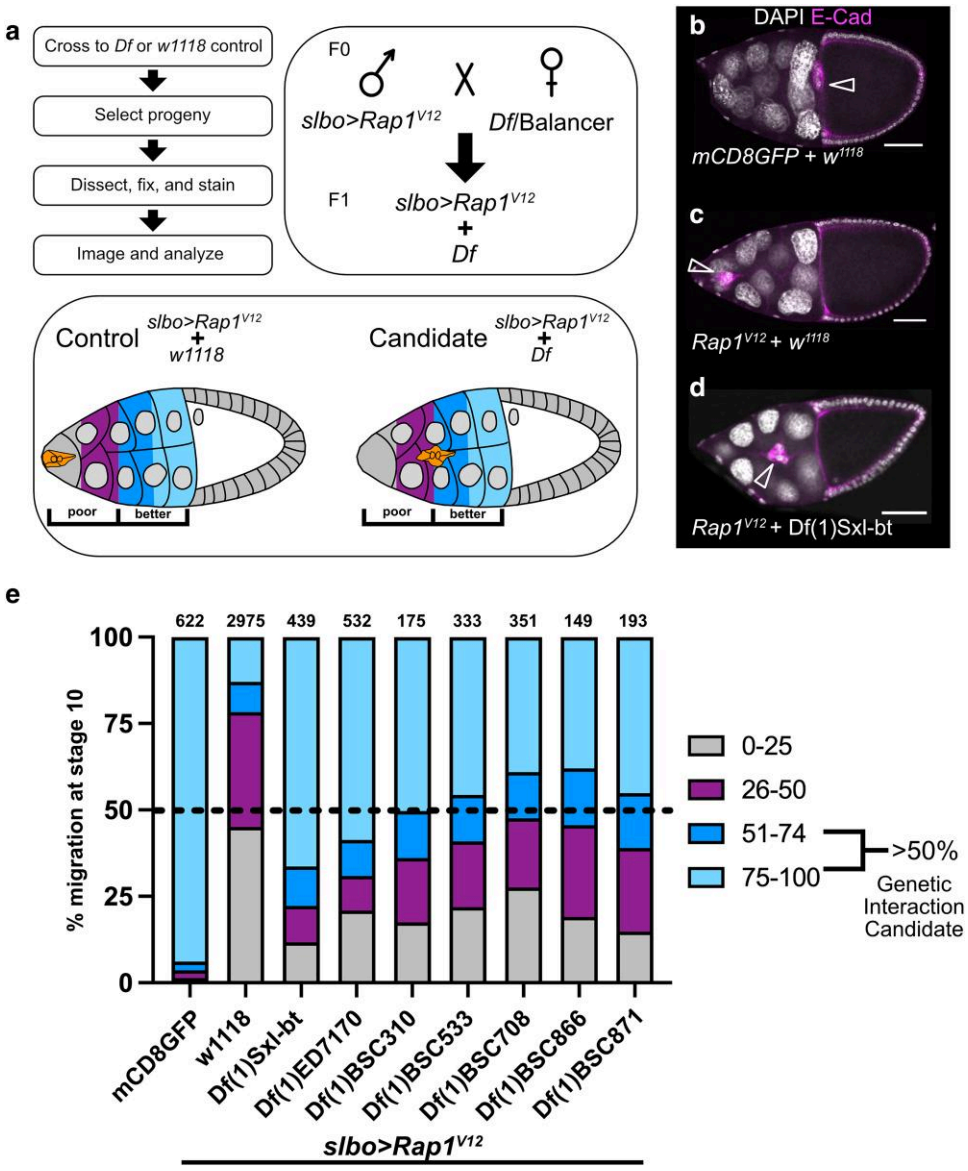

Fig. 1. Screen to identify *Rap1*^{V12} interacting regions. a) Screen design flow, crossing scheme, and egg chamber schematic showing border cell migration scoring criteria. Poor migration includes border cells found from the anterior tip of the egg chamber to the midway point to the oocyte (gray, 0–25% migration distance to the oocyte; magenta, 26–50% migration distance to oocyte). Better migration includes border cells found from the midway point to the oocyte (dark blue, 51–74% migration distance to the oocyte; light blue, 75–100% migration distance to the oocyte). b–d) Stage 10 egg chambers stained for E-cadherin (magenta) to label cell membranes and border cells (arrowheads) and DAPI to label cell nuclei (white). Scale bars, 50 μm. b) A representative *slbo* > *mCD8GFP* + w^{1118} control egg chamber showing border cells (arrowhead) that completed their migration at the oocyte. c) A representative *slbo* > *Rap1*^{V12} + w^{1118} egg chamber that failed to migrate and stopped at ~15% of the distance along the migration pathway. d) An example of a candidate dominant modifier of Rap1^{V12}. Here, *slbo* > *Rap1*^{V12} + *Df(1)Sxl-bt* (3196) border cells exhibit better migration but stopped at the egg chamber midpoint. e) Stacked bar chart displaying percent border cell migration at stage 10 for each of 7 candidate deficiency regions in a *slbo* > *Rap1*^{V12} background with *slbo* > *Rap1*^{V12} + w^{1118} and *slbo* > *mCD8GFP* + w^{1118} serving as controls. Numbers above each bar indicate the total egg chambers scored per genotype. Colors represent the border cell migration distance to the oocyte as depicted in a. The dashed line at 50% marks the screen hit threshold to be considered a genetic interaction candidate.

Results and discussion

A screen of the X chromosome for dominant modifiers of activated Rap1

Previous work demonstrated that regulated Rap1 activity is critical for its function in border cell migration and protrusion dynamics (Chang *et al.* 2018; Sawant *et al.* 2018). Expression of constitutively active Rap1 (*Rap1*^{V12}) specifically blocks border cell migration, causes ectopic protrusions, and alters the enrichment of E-Cadherin and F-actin within the cluster. These previous results demonstrate a requirement for Rap1 in generating productive directed protrusions and promoting the distribution of cell–cell adhesions during border cell migration. Rap1 interacts with the Hippo/Warts pathway in directed protrusions (Chang *et al.* 2018). While other Rap1 effectors likely mediate additional Rap1-dependent functions in border cells, their identities are unknown. Thus, here we performed a dominant modifier screen to identify additional Rap1-interacting genes in border cell migration. The X chromosome was chosen on the basis that chromosomes 2 and 3 had been screened previously for modifiers of constitutively activated Rap1^{V12} (Chang *et al.* 2018).

For the primary screen, we used the Bloomington Drosophila Stock Center (BDSC) X chromosome deficiency kit (DK1), which

Table 1. Primary screen results.

Symbol	BDSC[a] stock #	Breakpoints	Estimated Cytology	Hit[b] (Y, N, N[Ψ])	Fraction migrating ≤50%	Fraction migrating >50%	# Repeats	# EC[c] scored
Df(1)BSC843	27,887	X:254,968–255,277;X:334,685 (Df)	1A1;1A3 (Df)	N	70.49%	29.51%	1	122
Df(1)BSC530	25,058	X:364,350;X:623,478–623,577 (Df)	1A5;1B12 (Df)	N	73.21%	26.79%	1	56
Df(1)G1	34,050	X:644,873;X:654,238 (Df)	1B13;1B13 (Df)	N	66.95%	33.05%	2	214
Df(1)ED6443	9053	X:656,023;X:1,026,707 (Df)	1B14;1E1 (Df)	N[Ψ]	98.55%	1.45%	3	268
Df(1)BSC534	25,062	X:841,105;X:1,453,730 (Df)	1D1;2A3 (Df)	N	82.69%	17.31%	1	52
Df(1)BSC719	26,571	X:1,453,730;X:1,865,709 (Df)	2A3;2B13 (Df)	N[Ψ]	90.01%	9.99%	2	122
Df(1)BSC717	26,569	X:2,251,580;X:2,545,663 (Df)	2F2;3A4 (Df)	N[Ψ]	98.55%	1.45%	3	99
Df(1)ED411	8031	X:2,469,859;X:2,642,686 (Df)	3A3;3A8 (Df)	N	70.63%	29.38%	1	160
Df(1)ED6584	9348	X:2,636,213;X:2,685,435 (Df)	3A8;3B1 (Df)	N[Ψ]	97.26%	2.74%	3	199
Df(1)ED6630	8948	X:2,685,540;X:3,036,910 (Df)	3B1;3C5 (Df)	N[Ψ]	99.60%	0.40%	3	200
Df(1)BSC531	25,059	X:2,913,683–2,913,782;X:3,672,682 (Df)	3C3;3E2 (Df)	N	52.83%	47.17%	1	53
Df(1)BSC834	27,886	X:3,288,956;X:3,845,727 (Df)	3C11;3F3 (Df)	N[Ψ]	96.53%	3.47%	3	227
Df(1)ED6712	9169	X:3,432,535;X:3,789,615 (Df)	3D3;3F1 (Df)	N[Ψ]	94.74%	5.26%	2	96
Df(1)ED6716	24,145	X:3,799,196;X:4,204,584 (Df)	3F2;4B3 (Df)	N[Ψ]	94.54%	5.46%	3	242
Df(1)BSC580	25,414	X:4,101,232–4,101,613;X:4,688,080 (Df)	4A5;4C13 (Df)	N	69.83%	30.17%	2	102
Df(1)ED6727	8956	X:4,325,174;X:4,911,061 (Df)	4B6;4D5 (Df)	N	85.71%	14.29%	1	49
Df(1)JC70	944	X:4,679,537–4,919,558;X:5,309,242–5,412,386 (Df)	4C12-4D6;4F4-4F9 (Df)	N[Ψ]	95.98%	4.02%	2	177
Df(1)BSC533	25,061	X:5,282,581–5,282,584;X:5,428,543 (Df)	4F4;4F10 (Df)	Y	40.92%	59.08%	4	333
Df(1)Exel6235	7709	X:5,516,611;X:5,593,966 (Df)	5A2;5A6 (Df)	N	58.10%	41.90%	2	185
Df(1)BSC571	25,114	X:5,545,559;X:5,662,787 (Df)	5A4;5A10 (Df)	N	66.07%	33.93%	1	56
Df(1)ED6802	8949	X:5,679,980;X:5,965,880 (Df)	5A12;5D1 (Df)	N	56.07%	43.93%	2	172
Df(1)ED6829	8947	X:5,901,976;X:6,353,095 (Df)	5C7;5F3 (Df)	N	77.50%	22.50%	1	80
Df(1)Exel6239	7713	X:6,344,333;X:6,516,952–6,538,013 (Df)	5F2;6B1-6B2 (Df)	N	51.06%	48.94%	2	127
Df(1)Exel6240	7714	X:6,543,963;X:6,669,857–6,669,858 (Df)	6B2;6C4 (Df)	N	60.13%	39.87%	1	153
Df(1)BSC535	25,063	X:6,625,450;X:6,707,019 (Df)	6C2;6C8 (Df)	N	69.12%	30.88%	1	136
Df(1)BSC351	24,375	X:6,748,387–6,748,403;X:6,860,753 (Df)	6C11;6D7 (Df)	N[Ψ]	97.36%	2.64%	3	189
Df(1)BSC882	30,587	X:6,824,174;X:7,015,408 (Df)	6D3;6E4 (Df)	N	77.67%	22.33%	1	103
Df(1)BSC867	29,990	X:6,981,859;X:7,041,515 (Df)	6E4;6F1 (Df)	N	85.68%	14.32%	2	188
Df(1)Sxl-bt	3196	X:6,987,188–7,004,151;X:7,195,487–7,307,939 (Df)	6E4;7A3-7B1 (Df)	Y	22.20%	77.80%	5	439
Df(1)ED6906	8955	X:7,195,084;X:7,405,806 (Df)	7A3;7B2 (Df)	N	73.82%	26.18%	2	96
Df(1)BSC536	25,064	X:7,338,653;X:7,891,613 (Df)	7B2;7C1 (Df)	N	83.11%	16.89%	2	88
Df(1)C128	949	X:7,901,331–7,956,278;X:8,061,645–8,115,848 (Df)	7C2-7D1;7D5-7D6 (Df)	N	82.03%	17.97%	2	184
Df(1)BSC866	29,989	X:8,086,993;X:8,157,322 (Df)	7D5;7D16 (Df)	Y	45.61%	54.39%	3	149
Df(1)BSC662	26,514	X:8,116,248;X:8,489,613 (Df)	7D6;7F1 (Df)	N	50.63%	49.37%	3	270
Df(1)M38-C5	5706	X:8,877,627–8,933,650;X:9,554,623–9,594,143 (Df)	8B5-8C1;8E7-8E12 (Df)	N	69.70%	30.30%	1	33
Df(1)ED6957	8033	X:8,891,795;X:9,135,037 (Df)	8B6;8C13 (Df)	N	75.63%	24.37%	1	119
Df(1)BSC712	26,564	X:9,606,595;X:1,008,6569 (Df)	8F1;9B1 (Df)	N	76.02%	23.98%	3	186
Df(1)ED7005	9153	X:10,071,922;X:10,585,431 (Df)	9B1;9D3 (Df)	N[Ψ]	96.94%	3.06%	3	212
Df(1)BSC755	26,853	X:10,454,979;X:10,848,473 (Df)	9C4;9F5 (Df)	N	70.80%	29.20%	1	113
Df(1)BSC540	25,068	X:10,772,545;X:11,065,010 (Df)	9E8;10A3 (Df)	N	61.97%	38.03%	1	71
Df(1)v-L1	6219	X:10,854,869–10,925,631;X:11,108,482–11,136,887 (Df)	9F5-9F11;10A4-10A6 (Df)	N	74.60%	25.40%	1	63
Df(1)BSC572	25,391	X:10,890.940;X:11,092,253 (Df)	9F8;10A4 (Df)	N	78.03%	21.97%	1	132
Df(1)BSC287	23,672	X:11,182,121;X:11,426,241 (Df)	10A10;10B11 (Df)	N[Ψ]	99.62%	0.38%	3	299
Df(1)BSC722	26,574	X:11,350,466;X:11,754,251 (Df)	10B3;10E1 (Df)	N[Ψ]	93.00%	7.00%	2	89
Df(1)ED7147	9171	X:11714383;X:12004800 (Df)	10D6;11A1 (Df)	N[Ψ]	91.24%	8.76%	3	252
Df(1)ED7161	9217	X:12,007,087;X:12,750,866 (Df)	11A1;11B14 (Df)	N[Ψ]	93.11%	6.89%	3	247
Df(1)ED7170	8898	X:12,752,602;X:13,277,326 (Df)	11B15;11E8 (Df)	Y	30.90%	69.10%	7	532
Df(1)ED7225	24,146	X:13,784,406;X:14,322,206 (Df)	12C4;12E8 (Df)	N[Ψ]	100.00%	0.00%	1	61
Df(1)ED7229	9352	X:14,222,234;X:14,653,944 (Df)	12E5;12F2 (Df)	N	57.26%	42.74%	2	126
Df(1)ED7261	9218	X:14,653,809;X:14,839,412 (Df)	12F2;12F5 (Df)	N	87.67%	12.33%	5	424
Df(1)BSC310	24,336	X:14,842,413;X:15,089,556 (Df)	12F5;13A10 (Df)	Y	36.07%	63.93%	4	175
Df(1)ED7289	29732	X:15,024,777;X:15,125,750 (Df)	13A5;13A12 (Df)	N[Ψ]	96.48%	3.52%	5	543
Df(1)ED7294	8035	X:15,175,415;X:15,450,298 (Df)	13B1;13C3 (Df)	N	69.33%	30.67%	1	150
Df(1)ED7331	9219	X:15,450,255;X:15,813,523 (Df)	13C3;13F1 (Df)	N	87.50%	12.50%	3	239
Df(1)BSC714	26,566	X:15,758,351;X:16,086,028 (Df)	13E14;14A8 (Df)	N	81.08%	18.92%	1	37
Df(1)BSC758	26,855	X:16,005,260;X:16,367,112 (Df)	14A6;14C1 (Df)	N	53.67%	46.33%	2	191
Df(1)BSC772	26,869	X:16,302,976;X:16,423,105 (Df)	14B9;14C4 (Df)	N	75.21%	24.79%	1	117
Df(1)FDD-0024486	23,295	X:16,423,105;X:16,463,156 (Df)	14C4;14D1 (Df)	N	77.42%	22.58%	1	31
Df(1)BSC760	26,857	X:16,526,332;X:16,632,102 (Df)	14E1;14F2 (Df)	N	50.14%	49.86%	2	154
Df(1)BSC582	25,416	X:16,680,721;X:17,091,833 (Df)	15A1;15E2 (Df)	N	79.94%	20.06%	4	501
Df(1)ED7374	8954	X:16,695,187;X:17,107,632 (Df)	15A1;15E3 (Df)	N[Ψ]	91.33%	8.67%	3	253
Df(1)BSC405	24,429	X:17,830,759–17,830,846;X:18,092,832 (Df)	16D5;16F6 (Df)	N	83.33%	16.67%	1	30

(continued)

Table 1. (continued)

Symbol	BDSC[a] stock #	Breakpoints	Estimated Cytology	Hit[b] (Y, N, N$^{\Psi}$)	Fraction migrating ≤50%	Fraction migrating >50%	# Repeats	# EC[c] scored
Df(1)ED13478	29,733	X:18,085,406;X:18,102,011 (Df)	16F6;16F7 (Df)	N	88.55%	11.45%	2	218
Df(1)BSC352	24,376	X:18,117,467;X:18,374,885 (Df)	16F7;17A8 (Df)	N$^{\Psi}$	94.62%	5.38%	3	274
Df(1)BSC716	26,568	X:18,243,732;X:18,800,267 (Df)	17A3;17D6 (Df)	N	84.64%	15.36%	2	148
Df(1)ED7424	9350	X:18,657,253;X:19,298,773 (Df)	17D1;18C1 (Df)	N	86.87%	13.13%	2	147
Df(1)Exel7468	7768	X:19,264,512;X:19,509,637 (Df)	18B7;18C8 (Df)	N	75.00%	25.00%	1	52
Df(1)BSC275	23,171	X:19,496,689;X:19,580,079 (Df)	18C8;18D3 (Df)	N$^{\Psi}$	100.00%	0.00%	1	22
Df(1)BSC871	29,994	X:19,617,601;X:19,788,713 (Df)	18D7;18F2 (Df)	Y	38.96%	61.04%	4	193
Df(1)BSC586	25,420	X:19,788,713;X:20,429,928 (Df)	18F2;19D1 (Df)	N$^{\Psi}$	90.91%	9.09%	1	44
Df(1)BSC644	25,734	X:20,243,402;X:21,061,001 (Df)	19C1;19E7 (Df)	N	80.49%	19.51%	1	41
Df(1)DCB1-35b	977	X:20,939,503–21,345,088; X:22,980,722–23,542,271 (Df)	19E5-19F5;20F3-h32 (Df)	N	61.76%	38.24%	1	34
Df(1)BSC708	26,560	X:21,028,296;X:21,623,866 (Df)	19E7;20A4 (Df)	Y	47.56%	52.44%	5	351
Df(1)Exel6255	7723	X:21,519,203;X:22,517,665 (Df)	20A1;20C1 (Df)	N	50.22%	49.78%	4	390

[a] BDSC, Bloomington *Drosophila* Stock Center.
[b] Y, yes (suppressor); N, no (no interaction); N$^{\Psi}$, (possible enhancer).
[c] EC, egg chambers.

on aggregate deletes ~98% of the euchromatic *X* chromosome (Cook *et al.* 2012). Of the 93 lines within this kit, 19 lines were unable to be tested due to complicated genetics and/or health issues of the stocks. We crossed the remaining 74 female strains bearing the *X* chromosome deficiencies to males expressing UAS-*Rap1*^{V12} driven by the border cell-specific driver *slbo-GAL4* ("*slbo* > *Rap1*^{V12}"; Fig. 1a). Progeny expressing *Rap1*^{V12} driven by *slbo-GAL4* outcrossed to *w*^{1118} "wild type" background ("*slbo* > *Rap1*^{V12} + *w*^{1118}") exhibited very strong border cell migration defects (Fig. 1a, c, and e). By contrast, *slbo-GAL4* driven expression of UAS-*mCD8-GFP* in a *w*^{1118} background (*slbo* > *mCD8GFP* + *w1118*) resulted in normal migration (Fig. 1b and e). To quantify the Rap1^{V12} migration defect severity, we divided each egg chamber into four quadrants, 0–25, 26–50, 51–74, and 75–100% of the normal migration distance from the anterior egg chamber tip (0%) to the oocyte (100%; Fig. 1a and e). Relatively few *slbo* > *Rap1*^{V12} + *w*^{1118} border cell clusters traveled past the midpoint of migration (22% of egg chambers; Fig. 1a, c, and e). Therefore, we further simplified our scoring criteria by dividing the egg chamber into a region of "poor migration," defined as 0–50% of the migration distance before the midpoint of migration, and a region of "better migration," defined as 51–100% of the migration distance after the midpoint of migration (Fig. 1a). Using these criteria, we then performed the screen for deficiencies on the *X* chromosome that modified the *slbo* > *Rap1*^{V12} migration defects. While we identified enhancers of *Rap1*^{V12} migration defects (Table 1), these genes may represent more indirect regulators of Rap1 function. Therefore, we focused primarily on suppressors of *Rap1*^{V12}, which we reasoned were more likely to represent genes that function downstream of Rap1. We considered a screen hit as heterozygous loss of a deficiency that resulted in better migration in at least 50% of egg chambers assayed (Fig. 1a and e).

Using this screening approach, we identified 7 deficiency regions that dominantly suppressed the *slbo* > *Rap1*^{V12}-dependent migration defects (Fig. 1a, d, and e; Table 1). Each of these molecularly defined deficiencies completely or partially deletes an average of 9 genes, though some delete more genes (Cook *et al.* 2012). Using overlapping smaller deficiencies and publicly available mutant alleles and RNAi lines, we were able to map three of these regions to single interacting genes, which are described below.

Mapping the *Df(1)Sxl-bt* region reveals an interaction between *Rap1* and *fz4*

The strongest hit in this screen, *Df(1)Sxl-bt* (BDSC 3196), resulted in better migration in 78% of egg chambers analyzed (Fig. 1d and e; Table 1). This deficiency removes an estimated 191–321 kilobases (kb) of DNA (X:6,987,188–7,004,151 to X:7,195,487–7,307,939) along the *X* chromosome with a predicted deletion of 31 genes (FlyBase Öztürk-Çolak *et al.* 2024; Fig. 2a). We next used a smaller deficiency *Df(1)BSC867* (X:6,981,859 to X:7,041,515) to further refine the gene region (FlyBase; Fig. 2a). Border cell clusters expressing *slbo* > *Rap1*^{V12} and heterozygous for *Df(1)BSC867* migrated past the midpoint only 14% of the time, similar to *slbo* > *Rap1*^{V12} + *w*^{1118} alone (Fig. 2c). We therefore considered it unlikely that Rap1-interacting genes resided within this segment of *Df(1)Sxl-bt*. We next focused on the region extending from the end of *Df(1)BSC867* to the end of *Df(1)Sxl-bt* (X:7,041,515-X:7,307,939). As there were no available deficiencies that overlapped with this region, we next tested for interaction with mutant alleles of characterized genes within the breakpoint region. Only 2 genes within this region, *Sex lethal* (*Sxl*) and *frizzled 4* (*fz4*) had characterized loss of function mutant alleles. Therefore, we tested the interaction of Sxl^{f2} and *fz4*$^{3-1}$ with Rap1^{V12}. Border cells migrated past the midpoint in only 1% of *slbo* > *Rap1*^{V12} + Sxl^{f2} egg chambers (Fig. 2c). In contrast, border cells in *slbo* > *Rap1*^{V12} + *fz4*$^{3-1}$ egg chambers migrated significantly better, with 46% of clusters migrating past the midpoint compared with 18% in matched *slbo* > *Rap1*^{V12} + *w*^{1118} controls (Fig. 2b and c; Table 2; $P < 0.0001$, Chi-squared test).

Single-cell RNA sequencing data from the Fly Cell Atlas project revealed the expression of *fz4* in both somatic and germline cells of the ovary, indicating that *fz4* is expressed in the relevant tissue (Li *et al.* 2022). Additionally, *fz4* transcript is differentially expressed during border cell migration (Burghardt *et al.* 2023). To determine whether *fz4* is required for border cell migration, we targeted *fz4* with RNAi using 2 independent, nonoverlapping RNAi lines (*fz4* RNAi #1 BDSC 64990 and *fz4* RNAi #2 VDRC 102339), each of which was expressed under the control of a strong early follicle cell and border cell driver, *c306-GAL4* (Manseau *et al.* 1997). *c306-GAL4* driven expression of a nonessential RNAi targeting GFP ("GFP RNAi") resulted in normal migration, or ≥75% of the distance to the oocyte (Fig. 2d). Therefore, we considered any border cell

Table 2. Candidate allele raw results and statistics.

Allele	Total egg chambers (N)	Number of egg chambers with border cells migrating >50% (N)	Statistical test	Significance
fz4[3-1]	393	180	Chi-square test	$P < 0.0001$
Matched control	287	49		
Usp16-45[B]	292	159	Chi-square test	$P < 0.0001$
Matched control	354	64		
sno[EF531]	525	198	Chi-square test	$P < 0.0001$
Matched control	411	67		
Su(H)[2]	410	173	Chi-square test	$P < 0.0001$
Matched control	287	49		

N, number of egg chambers scored.

Table 3. Candidate gene RNAi raw results and statistics.

RNAi Line (stock)/Gene	Total egg chambers (N)	Number of egg chambers with border cells migrating <75% (N)	Statistical test	Significance
64,990 *fz4* RNAi #1[a]	238	0	Chi-square test	$P < 0.01$
60,102 matched control[b]	202	9		
102,339 *fz4* RNAi #2[b]	186	9	Chi-square test	ns
60,102 matched control[b]	239	9		
41,976 *Usp16-45* RNAi #1[b]	152	35	Chi-square test	$P < 0.0001$
60,102 matched control[b]	239	9		
110,286 *Usp16-45* RNAi #2[b]	196	4	Chi-square test	ns
60,102 matched control[b]	239	9		
28,341 *sno* RNAi #1[b]	185	28	Chi-square test	$P < 0.0001$
60,102 matched control[b]	239	9		
10,1404 *sno* RNAi #2[b]	109	39	Chi-square test	$P < 0.0001$
60,102 matched control[b]	259	9		

N, number of egg chambers scored.
[a] BDSC stock.
[b] VDRC stock.

clusters that failed to reach the oocyte (≤74% of the migration distance), as having a migration defect. *fz4* RNAi #1 resulted in normal migration, with all border cells migrating ≥75% of the distance to the oocyte (Fig. 2d). Similarly, *fz4* RNAi #2 resulted in a minimal 5% migration defect that resembled the 3% defect observed in GFP RNAi controls (Fig. 2d; Table 3). These data suggest that *fz4* on its own may be dispensable for the ability of border cells to complete their migration to the oocyte.

Fz4 is a member of the Frizzled family of proteins that act as receptors for secreted Wnt proteins (Huang and Klein 2004). Wnt inhibitor of Dorsal (WntD/Wnt8) and Wnt4 both bind Fz4 (Wu and Nusse 2002; Gordon *et al.* 2005; McElwain *et al.* 2011). WntD functions in the Toll-Dorsal pathway to pattern the gastrulating embryo but has limited expression in ovarian follicle cells (Ganguly *et al.* 2005; Rahimi *et al.* 2016; Li *et al.* 2022). Wnt4, however, contributes to cell movement in the pupal ovary and is required for border cell migration (Cohen *et al.* 2002; Kotian *et al.* 2022). The role for Wnt4 in border cell migration thus may be independent of Fz4. RNAi for Fz4 did not impair migration, with the caveat that the knockdown efficiency may be incomplete. Alternatively, Wnt4 could bind multiple Frizzled proteins to coordinate its function in border cell migration. Indeed, in *Drosophila* S2 cells, Wnt4 binds to both Fz and Fz2 in addition to Fz4 (Wu and Nusse 2002). Both Fz2 and Fz4 are differentially expressed in border cells (Burghardt *et al.* 2023). Thus, Fz2 and Fz4 could function redundantly or together in border cells, though this remains to be formally tested.

Currently, it is unclear how *fz4* heterozygosity modifies the $Rap1^{V12}$ border cell migration defect. Notably, $Rap1^{V12}$ border cell clusters accumulate excessive E-Cadherin at the cluster periphery (Sawant *et al.* 2018). Low levels of E-cadherin at the cluster periphery provide optimal traction of border cells upon the nurse cell substrate for forward movement (Niewiadomska *et al.* 1999; Cai *et al.* 2014). Wnt4 regulates focal adhesion kinase (FAK) in the pupal ovary, a component of integrin-based focal adhesions (Cohen *et al.* 2002; Chastney *et al.* 2025). While Rap1 can regulate integrins in various cell types, FAK is not required for border cell migration and integrins appear to play minor roles in cluster organization (Grabbe *et al.* 2004; Llense and Martín-Blanco 2008; Sun *et al.* 2022). It is possible that Wnt4, through Fz4 and possibly other Frizzled receptors, regulates multiple types of adhesions in migratory border cells (Kotian *et al.* 2022). Loss of *fz4*, therefore, could be sufficient to modify the adhesion defects caused by $Rap1^{V12}$, but insufficient to cause border cell migration defects on its own.

Mapping the *Df(1)BSC533* region reveals an interaction between *Rap1* and *Usp16-45*

Border cell clusters expressing *slbo* > $Rap1^{V12}$ and heterozygous for *Df(1)BSC533* (BDSC 25061) migrated past the migration midpoint 59% of the time (Fig. 1e; Table 1). *Df(1)BSC533* deletes approximately 146 kb of DNA (X:5,282,581–5,282,584 to X:5,428,543) along the *X* chromosome and results in the predicted deletion of 21 genes (FlyBase; Fig. 3a). Two overlapping deficiencies, *Df(1)BSC823* (BDSC 27584; X:5,282,581 to X:5,332,808) and *Df(1)Exel6290* (BDSC 7753; X:5,364,532 to 5,428,543), each interacted with *slbo* > $Rap1^{V12}$ (FlyBase; Fig. 3a and d). While these 2 smaller deficiencies do not themselves overlap, the interaction with *Df(1)Exel6290* was stronger. Therefore, we focused on the *Df(1)Exel6290* region, which deletes 6 genes including *Ubiquitin-specific protease 16/45* (*Usp16-45*;Fig. 3a). A point mutation allele for this gene, $Usp16\text{-}45^{[B]}$, was able to partially replicate the interaction observed for this deficiency with $Rap1^{V12}$. Border cells migrated past the midpoint in 52% of *slbo* > $Rap1^{V12}$ + $Usp16\text{-}45^{[B]}$ egg chambers, compared with 19% in

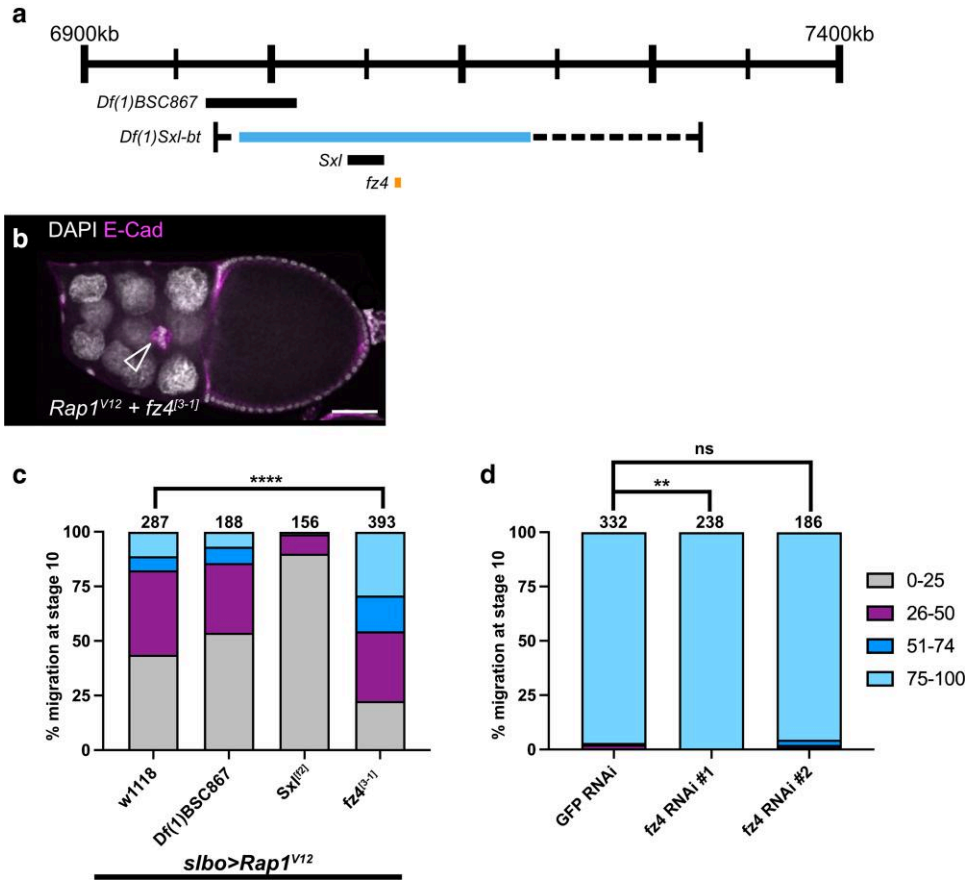

Fig. 2. *Fz4* lies within *Df(1)Sxl-bt* and interacts with $Rap1^{V12}$. a) Schematic genomic region illustrating the location of *fz4* within *Df(1)Sxl-bt* along with overlapping deficiencies and genes tested. The numbers refer to the genomic location of the deficiency. b) A stage 10 $Rap1^{V12}$ + $fz4^{[3-1]}$ egg chamber with border cells (arrowhead) that have moved past 50% of the egg chamber length. E-cadherin (magenta) labels all cell membranes including the border cells and DAPI labels cell nuclei (white). Scale bar, 50 μm. c) Stacked bar chart displaying border cell migration for *slbo* > $Rap1^{V12}$ + w^{1118}, *slbo* > $Rap1^{V12}$ + *Df(1)BSC867* (BDSC 29990), *slbo* > $Rap1^{V12}$ + $Sxl^{[f2]}$ (BDSC 4593), and *slbo* > $Rap1^{V12}$ + $fz4^{[3-1]}$ (BDSC 38412). Numbers above each bar indicate the total egg chambers scored per genotype. **** $P < 0.0001$, 2-sided Chi-square test. Data for *slbo* > $Rap1^{V12}$ + *Df(1)BSC867* (BDSC 29990) and *slbo* > $Rap1^{V12}$ + $Sxl^{[f2]}$ (BDSC 4593) are from the original mapping results and are shown here for simplicity. The statistical test was performed only between *slbo* > $Rap1^{V12}$ + $fz4^{[3-1]}$ (BDSC 38412) and the matched *slbo* > $Rap1^{V12}$ + w^{1118} control (Table 2). d) Stacked bar chart displaying border cell migration for *c306-GAL4* > *GFP* RNAi (VDRC 60102), *c306-GAL4* > *fz4* RNAi#1 (BDSC 64990), and *c306-GAL4* > *fz4* RNAi#2 (VDRC 102339). Numbers above each bar indicate the total egg chambers scored per genotype. ** $P < 0.001$, 2-sided Chi-square test; ns, not significant, 2-sided Chi-square test. Cumulative *c306-GAL4* > *GFP* RNAi (VDRC 60102) data for this experiment is shown for simplicity, but statistical tests were performed between the matched experimental and control data (Table 3).

matched *slbo* > $Rap1^{V12}$ + w^{1118} controls (Fig. 3b and d; Table 2; $P < 0.0001$, Chi-squared test).

Usp16-45 is a member of the ubiquitin-specific proteases (USP) subfamily of deubiquitinases (Clague *et al.* 2019). While Usp16-45 has no known roles in cell migration, the family member *nonstop* (*not*), a USP22 ortholog, is required for border cell migration (Badmos *et al.* 2021). Single-cell RNA sequencing data from the Fly Cell Atlas project revealed the expression of *Usp16-45* in both somatic and germline cells of the ovary, indicating that *Usp16-45* is expressed in the relevant tissue (Li *et al.* 2022). *Usp16-45* is also differentially expressed in migrating border cells (Burghardt *et al.* 2023). To determine whether Usp16-45 is required for border cell migration, we expressed RNAi lines targeting the gene under the control of *c306*-GAL4. Two independent, nonoverlapping RNAi constructs (*Usp16-45* RNAi #1 VDRC 41976 and *Usp16-45* RNAi #2 VDRC 110286) provided mixed results. *Usp16-45* RNAi #1 resulted in moderately strong migration defects, with 24% of border cell clusters failing to reach the oocyte by stage 10 (Fig. 3c and e; Table 3). This value is significantly different than the 3% defect observed in controls (Fig. 3e; Table 3; $P < 0.0001$, Chi-squared test). *Usp16-45* RNAi #2, however, resulted in minimal (2%) migration defects (Fig. 3e; Table 3). Although *Usp16-45* RNAi #2 failed to impact migration, it is possible that *Usp16-45* RNAi #1 results in more efficient knockdown of *Usp16-45*. Furthermore, no off-targets are predicted for *Usp16-45* RNAi #1, suggesting that the phenotypes observed are produced by specific knockdown of *Usp16-45* (Hu *et al.* 2013). Given the dominant genetic interaction of a *Usp16-45* mutant allele with $Rap1^{V12}$ and the phenotypes caused by *Usp16-45* RNAi#1, we conclude that *Usp16-45* genetically interacts with Rap1 and is required for border cell migration.

Usp16-45 has predicted cysteine-type deubiquitinase activity (FlyBase; Komander *et al.* 2009). Small GTPases like Rap1 are often regulated by posttranslational modifications (Konstantinopoulos *et al.* 2007). Posttranslational modification at the CAAX domain, for example, can facilitate membrane targeting of GTPases (Konstantinopoulos *et al.* 2007). Ubiquitination is a mode of posttranslational modification that can regulate small GTPase stability, activity, and localization (Lei *et al.* 2021). However, it is currently unclear whether Usp16-45 directly targets Rap1. RAPGEF2, an activating GEF for Rap1, is known to be targeted for ubiquitination (Kim *et al.* 2015). The RAPGEF2 ortholog PDZ-GEF (also known as Dizzy) is required for border cell migration, though

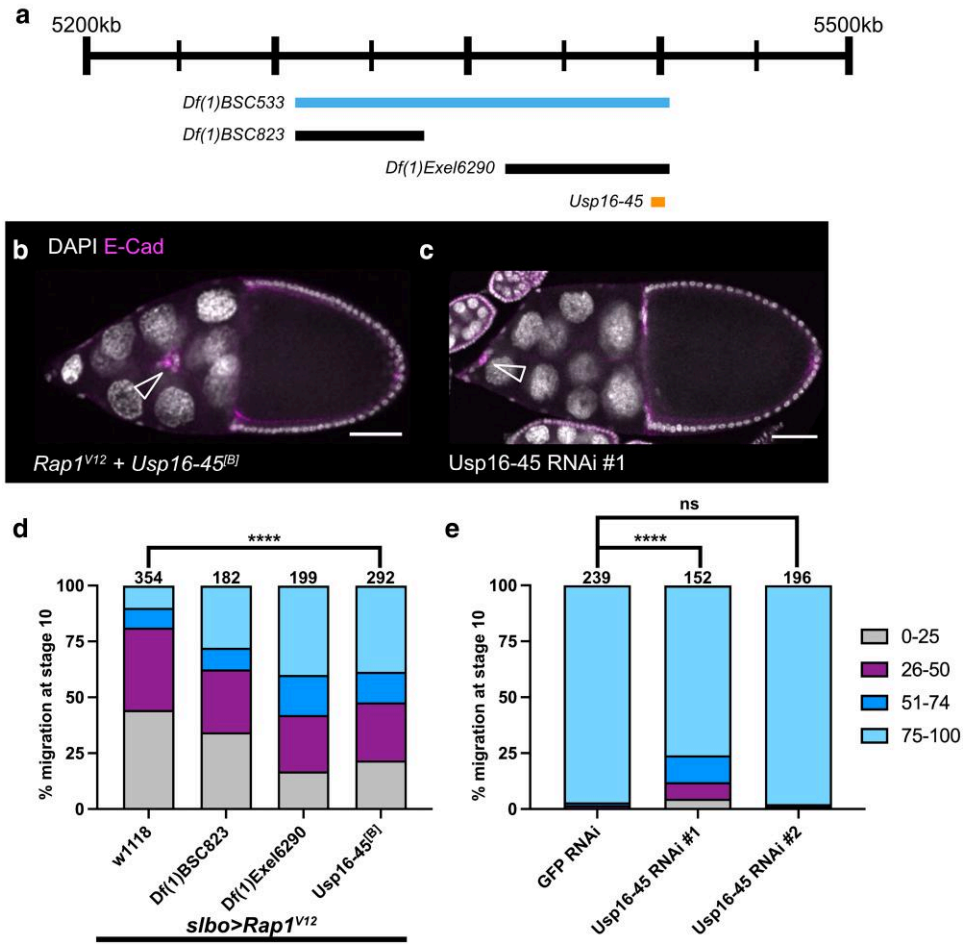

Fig. 3. *Usp16-45* lies within *Df(1)BSC533*, interacts with $Rap1^{V12}$, and is required for border cell migration. a) Schematic genomic region illustrating where *Usp16-45* lies within *Df(1)BSC533* along with overlapping deficiencies tested. b,c) Stage 10 egg chambers stained for E-cadherin (magenta), which labels all cell membranes including the border cells and DAPI to label cell nuclei (white). Arrowheads indicate border cell clusters. Scale bars, 50 μm. b) A $Rap1^{V12}$ + $Usp16\text{-}45^{[B]}$ egg chamber showing with border cells (arrowhead) moving past 50% of the egg chamber length. c) A *c306-GAL4* > *Usp16-45* RNAi #1 (VDRC 41976) egg chamber with a strong border cell migration defect. d) Stacked bar chart displaying border cell migration for *slbo* > $Rap1^{V12}$ + w^{1118}, *slbo* > $Rap1^{V12}$ + *Df(1)BSC823* (BDSC 27584), *slbo* > $Rap1^{V12}$ + *Df(1)Exel6290* (BDSC 7753), and *slbo* > $Rap1^{V12}$ + $Usp16\text{-}45^{[B]}$ (BDSC 57080). Numbers above each bar indicate the total egg chambers scored per genotype. **** $P < 0.0001$, 2-sided Chi-square test. Data for *slbo* > $Rap1^{V12}$ + *Df(1)BSC823* (BDSC 27584) and *slbo* > $Rap1^{V12}$ + *Df(1)Exel6290* (BDSC 7753) are from the original mapping approach and shown here for simplicity. The statistical test was performed only between *slbo* > $Rap1^{V12}$ + $Usp16\text{-}45^{[B]}$ (BDSC 57080) and *slbo* > $Rap1^{V12}$ + w^{1118} matched control (Table 2). e) Stacked bar chart displaying border cell migration for *c306-GAL4* > *GFP* RNAi (VDRC 60102), *c306-GAL4* > *Usp16-45* RNAi #1 (VDRC 41976), and *c306-GAL4* > *Usp16-45* RNAi #2 (VDRC 110286). Numbers above each bar indicate the total egg chambers scored per genotype. **** $P < 0.0001$, 2-sided Chi-square test; ns, not significant, 2-sided Chi-square test (Table 3).

a role for ubiquitination has not been tested (Sawant *et al.* 2018). These data suggest that the addition or removal of ubiquitin could be critical in regulating Rap1 signaling in border cells. Further work will be required to determine if Usp16-45 targets Rap1 directly, or indirectly via regulation of a signaling partner such as PDZ-GEF or another Rap1-interacting protein.

Mapping the *Df(1)ED7170* region reveals an interaction between *Rap1* and *sno*

Border cell clusters expressing *slbo* > $Rap1^{V12}$ and heterozygous for *Df(1)ED7170* (BDSC 8898) migrated past the midpoint in 69% of egg chambers (Fig. 1e; Table 1). *Df(1)ED7170* deletes approximately 525 kb of DNA (X:12,752,602 to X:13,277,326) along the *X* chromosome (FlyBase; Fig. 4a) and interacted strongly with *slbo* > $Rap1^{V12}$. *Df(1)ED7170* is predicted to delete or disrupt 60 genes. Using deficiencies *Df(1)ED7165* (BDSC 9058; X:12,752,602 to X:13,138,948) and *Df(1)BSC713* (BDSC 26565; X:13,159,870 to X:13,373,704) led us to focus on the region extending from X:13,159,870 to X:13,277,326, which covers the beginning of *Df(1)BSC713* to the end of *Df(1)ED7170* (FlyBase; Fig. 4a and h). Using available alleles of genes within this region led us to investigate the gene *strawberry notch* (*sno*). Sno is a nuclear protein that functions in Notch signaling (Majumdar *et al.* 1997). Single-cell RNA sequencing data from the Fly Cell Atlas project indicates *sno* expression in both the germline and somatic cells of the ovary (Li *et al.* 2022). Using a GFP protein trap in *sno*, $sno^{CC01032}$, we found that Sno is found in the nuclei of all cells including the nurse cells, follicle cells, and border cells (Fig. 4b and b′).

We were able to partially replicate the interaction observed for *Df(1)ED7170* with a loss of function allele for *sno*, sno^{EF531}. Border cells migrated past the midpoint in 37% of egg chambers scored for *slbo* > $Rap1^{V12}$ + sno^{EF531} compared with 17% in controls (Fig. 4d and h; Table 2; $P < 0.0001$, Chi-squared test). Genetic interaction experiments in the wing and eye place *sno* in the Notch pathway (Coyle-Thompson and Banerjee 1993). Rough eye and wing notching phenotypes found in *sno* mutants are rescued by

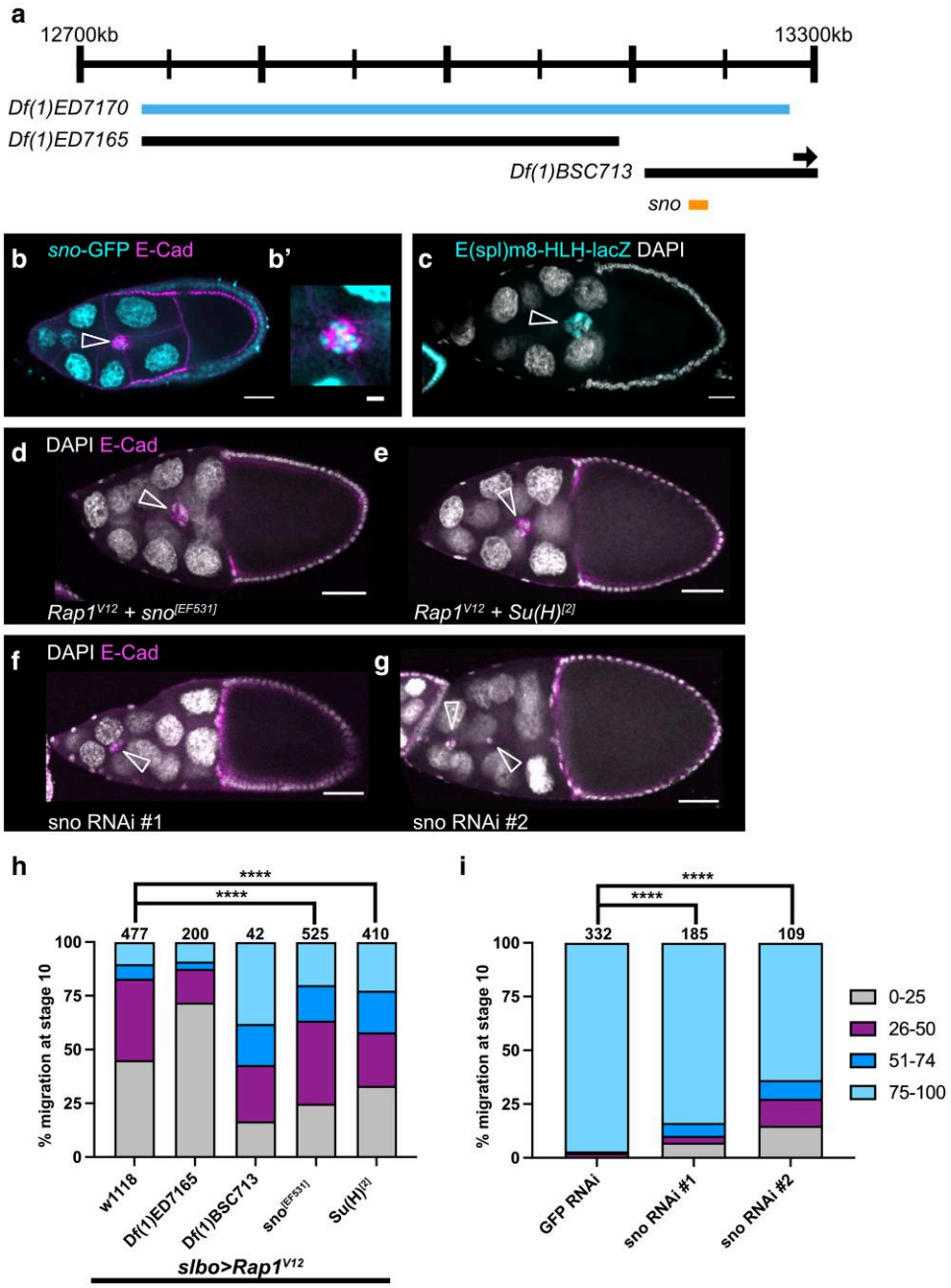

Fig. 4. *Sno* lies within *Df(1)ED7170*, interacts with $Rap1^{V12}$, and is required for border cell migration. a) Schematic genomic region illustrating where *sno* lies within *Df(1)ED7170* along with overlapping deficiencies tested. Arrow indicates that *Df(1)BSC713* extends beyond the genomic region depicted here. b) Egg chamber with GFP protein trap in *sno*, $sno^{CC01032}$, shows Sno nuclear expression (cyan). E-cadherin (magenta) labels cell membranes including the border cells. (B') Close-up view of the same border cell cluster in b. c) Egg chamber with Notch activity reporter, *E(spl)m8-HLH-lacZ* (also known as Su(H)-lacZ), which shows nuclear expression in border cells (cyan). DAPI (white) labels cell nuclei. d–g) Stage 10 egg chambers stained for E-cadherin (magenta), which labels all cell membranes including the border cells and DAPI to label cell nuclei (white). d) A $Rap1^{V12}$ + $sno^{[EF531]}$ egg chamber with the border cells moving past 50% of the egg chamber length. e) A $Rap1^{V12}$ + $Su(H)^{[2]}$ egg chamber with the border cells moving past 50% of the egg chamber length. f) A *c306-GAL4* > *Sno* RNAi #1 (VDRC 28341) egg chamber with a strong border cell migration defect. g) A *c306-GAL4* > *Sno* RNAi #2 (VDRC 101404) egg chamber with a strong border cell migration defect. b–g) Arrowheads indicate border cell clusters. Scale bars, 20 μm (b and c), 5 μm (b'), and 50 μm (d–g). h) Stacked bar chart displaying border cell migration for *slbo* > $Rap1^{V12}$ + w^{1118}, *slbo* > $Rap1^{V12}$ + *Df(1)ED7165* (BDSC 9058), *slbo* > $Rap1^{V12}$ + *Df(1)BSC713* (BDSC 26565), *slbo* > $Rap1^{V12}$ + $sno^{[EF531]}$ (BDSC 33833), and *slbo* > $Rap1^{V12}$ + $Su(H)^{[2]}$ (BDSC 30477). Numbers above each bar indicate the total egg chambers scored per genotype. **** $P < 0.0001$, 2-sided Chi-square test. Data for *slbo* > $Rap1^{V12}$ + *Df(1)ED7165* (BDSC 9058) and *slbo* > $Rap1^{V12}$ + *Df(1)BSC713* (BDSC 26565) are from the original mapping approach and shown here for simplicity. Statistical tests were performed only between *slbo* > $Rap1^{V12}$ + $sno^{[EF531]}$ (BDSC 33833) and *slbo* > $Rap1^{V12}$ + w^{1118} matched control or *slbo* > $Rap1^{V12}$ + $Su(H)^{[2]}$ (BDSC 30477) and *slbo* > $Rap1^{V12}$ + w^{1118} matched control (Table 2). i) Stacked bar chart displaying border cell migration for *c306-GAL4* > *GFP* RNAi (VDRC 60102), *c306-GAL4* > *sno* RNAi #1 (VDRC 28341), and *c306-GAL4* > *sno* RNAi #2 (VDRC 101404). Numbers above each bar indicate the total egg chambers scored per genotype. **** $P < 0.0001$, 2-sided Chi-square test. Cumulative *c306-GAL4* > *GFP* RNAi (VDRC 60102) data for this experiment was reported for simplicity, but statistical tests were performed between matched experimental and control data (Table 3).

an extra copy of *Notch* (Coyle-Thompson and Banerjee 1993). Similarly, combining the hypomorphic nd^1 allele of *Notch* with the temperature-sensitive sno^{71e3} allele synergistically enhances the mild wing phenotypes present in nd^1 alone (Coyle-Thompson and Banerjee 1993). Sno also binds to Suppressor of Hairless [Su(H)] downstream of Epidermal Growth Factor Receptor (EGFR) signaling in *Drosophila* eye development (Tsuda *et al.* 2002). Notch activity, as visualized by a lacZ reporter containing both Su(H) and Grainyhead (Grh) binding sites, E(spl)m8-HLH-lacZ, is high in migrating border cells (Fig. 4c; Furriols and Bray 2001; Schober *et al.* 2005; Wang *et al.* 2007). Therefore, to determine if the interaction between *sno* and $Rap1^{V12}$ is related to Sno-dependent regulation of Su(H), we next tested a *Su(H)* loss of function allele, $Su(H)^{[2]}$. Border cells migrated past the midpoint in 42% of *slbo* > $Rap1^{V12}$ + $Su(H)^{[2]}$ egg chambers compared with 17% in *slbo* > $Rap1^{V12}$ + w^{1118} controls (Fig. 4e and h; Table 2). These results indicate that *sno* and *Su(H)* both interact with Rap1 in border cell migration, possibly through their roles in the Notch pathway.

We next asked whether *sno* was essential for border cell migration on its own. Prior work indicates a role for Sno in successful oogenesis. Females homozygous for the *sno* allele sno^{71e1} had severe defects in oogenesis including a reduced number of ovarioles, dying egg chambers, and disrupted egg chamber polarity (Coyle-Thompson and Banerjee 1993). To determine whether *sno* is required specifically for border cell migration, we targeted *sno* with RNAi lines expressed under the control of the follicle cell driver *c306-GAL4*. Using 2 independent, nonoverlapping constructs (*sno* RNAi #1 VDRC 28341 and *sno* RNAi #2 VDRC 101404), we found that *sno* is required for migration (Fig. 4f, g, and i). *sno* RNAi #1 resulted in a significant migration defect of 16% (Fig. 4f and i; Table 3). Similarly, we observed 36% migration defects for *sno* RNAi #2 (Fig. 4g and i; Table 3). The difference in migration defects between RNAi lines is likely due to differences in knockdown efficiency.

How *sno* and *Su(H)* contribute to border cell migration via the Rap1 pathway is unclear. Notch and its ligand Delta are required for normal border cell migration (Schober *et al.* 2005; Wang *et al.* 2007). Both active Notch and *Su(H)* are expressed during migration (Fig. 4c; Wang *et al.* 2007). One downstream target of Notch-Su(H) is Anterior open (Aop, also known as Yan; Schober *et al.* 2005). Aop regulates the turnover of E-Cadherin required for efficient border cell migration (Schober *et al.* 2005). One possibility is that Sno could regulate Aop, which in turn impacts migration efficiency via E-Cadherin turnover. The interaction between *sno* and $Rap1^{V12}$ could thus be explained by a common target, E-Cadherin. Further work will be required to determine if this hypothesis is supported, or if another mechanism is at play.

Conclusions

The goal of this screen was to identify molecular partners and potential effectors of Rap1 GTPase activity that are relevant for collective cell migration. Here, we report 7 deficiency regions that genetically interacted with *slbo* > $Rap1^{V12}$. Of these 7 regions, three were mapped to single genes. Fz4, Usp16-45, and Sno may function as effectors of Rap1 GTPase or act as parallel factors that similarly regulate border cell migration. *Sno* and *Usp16-45* were each required for border cell migration on their own, while *fz4* was not. It is important to note that heterozygous loss of these genes did not completely recapitulate the interaction of the relevant deficiency with $Rap1^{V12}$. This could be due to the heterozygous loss of additional genes in these genomic regions that interact with Rap1 or because of the nature of the mutant alleles used. Additional work will be needed to determine which of these 2 possibilities is most likely. Rap1 functions autonomously in border cells to promote collective cell migration (Chang *et al.* 2018; Sawant *et al.* 2018). However, we cannot rule out nonautonomous suppression of $Rap1^{V12}$ border cell migration defects by heterozygous loss of one or more of the deficiency regions from the germline-derived nurse cells. Therefore, future identification of the relevant genes from the four other interacting deficiencies, in border cells and/or in nurse cells, is expected to yield additional Rap1 effectors and interacting genes. In sum, this unbiased genetic modifier screen identified multiple genes that interact with Rap1 during border cell migration. Follow-up studies will be needed to fully characterize how each gene cooperates with Rap1 to facilitate border cell migration and determine if these genes function in other types of collectively migrating cells during development and in cancer.

Data availability

Drosophila strains are available upon request. The authors affirm that all data necessary for confirming the conclusions of the article are present within the article, figures, and tables. Table 1 contains the complete results of the screen. Table 2 shows the raw results and statistics of the genetic interaction tests with mutant alleles and Table 3 shows the raw results and statistics of the RNAi knockdown tests in border cells.

Acknowledgments

We would like to thank the Bloomington Drosophila Stock Center (NIH P40OD018537) and the Vienna Drosophila Resource Center for providing flies, and the Developmental Studies Hybridoma Bank, created by the NICHD of the NIH and maintained at the University of Iowa, for providing antibodies used in this study. We used FlyBase (release FB2024_03) for information on genes, functions, and stocks. We also thank the Kansas State University Confocal Core for use of the Zeiss LSM880 confocal.

Funding

This work was supported by a grant from the National Science Foundation, United States, (NSF 2027617) to J.A.M. and by Johnson Cancer Research Center, Kansas State University, Graduate Student Summer Stipend Awards to C.L.M., E.B., and J.A.M.

Conflicts of interest

The authors declare no conflict of interest.

Literature cited

Aranjuez G, Burtscher A, Sawant K, Majumder P, McDonald JA. 2016. Dynamic myosin activation promotes collective morphology and migration by locally balancing oppositional forces from surrounding tissue. Mol Biol Cell. 27(12):1898–1910. doi:10.1091/mbc.e15-10-0744.

Badmos H, Cobbe N, Campbell A, Jackson R, Bennett D. 2021. *Drosophila* USP22/nonstop polarizes the actin cytoskeleton during collective border cell migration. J Cell Biol. 220(7):e202007005. doi:10.1083/jcb.202007005.

Boettner B, Van Aelst L. 2009. Control of cell adhesion dynamics by Rap1 signaling. Curr Opin Cell Biol. 21(5):684–693. doi:10.1016/j.ceb.2009.06.004.

Bonello TT, Perez-Vale KZ, Sumigray KD, Peifer M. 2018. Rap1 acts via multiple mechanisms to position Canoe and adherens junctions and mediate apical-basal polarity establishment. Development. 145(2):dev157941. doi:10.1242/dev.157941.

Bromberger T, Klapproth S, Rohwedder I, Weber J, Pick R, Mittmann L, Min-Weißenhorn SJ, Reichel CA, Scheiermann C, Sperandio M, *et al.* 2021. Binding of Rap1 and Riam to Talin1 Fine-Tune β2 integrin activity during leukocyte trafficking. Front Immunol. 12:702345. doi:10.3389/fimmu.2021.702345.

Burghardt E, Rakijas J, Tyagi A, Majumder P, Olson BJSC, McDonald JA. 2023. Transcriptome analysis reveals temporally regulated genetic networks during *Drosophila* border cell collective migration. BMC Genomics. 24(1):728. doi:10.1186/s12864-023-09839-8.

Cai D, Chen SC, Prasad M, He L, Wang X, Choesmel-Cadamuro V, Sawyer JK, Danuser G, Montell DJ. 2014. Mechanical feedback through E-cadherin promotes direction sensing during collective cell migration. Cell. 157(5):1146–1159. doi:10.1016/j.cell.2014.03.045.

Chang Y-C, Wu J-W, Hsieh Y-C, Huang T-H, Liao Z-M, Huang Y-S, Mondo JA, Montell D, Jang AC-C. 2018. Rap1 negatively regulates the hippo pathway to polarize directional protrusions in collective cell migration. Cell Rep. 22(8):2160–2175. doi:10.1016/j.celrep.2018.01.080.

Chastney MR, Kaivola J, Leppänen V-M, Ivaska J. 2025. The role and regulation of integrins in cell migration and invasion. Nat Rev Mol Cell Biol. 26(2):147–167. doi:10.1038/s41580-024-00777-1.

Cherfils J, Zeghouf M. 2013. Regulation of small GTPases by GEFs, GAPs, and GDIs. Physiol Rev. 93(1):269–309. doi:10.1152/physrev.00003.2012.

Clague MJ, Urbé S, Komander D. 2019. Breaking the chains: deubiquitylating enzyme specificity begets function. Nat Rev Mol Cell Biol. 20(6):338–352. doi:10.1038/s41580-019-0099-1.

Cohen ED, Mariol M-C, Wallace RMH, Weyers J, Kamberov YG, Pradel J, Wilder EL. 2002. DWnt4 regulates cell movement and focal adhesion kinase during *Drosophila* ovarian morphogenesis. Dev Cell. 2(4):437–448. doi:10.1016/S1534-5807(02)00142-9.

Cook RK, Christensen SJ, Deal JA, Coburn RA, Deal ME, Gresens JM, Kaufman TC, Cook KR. 2012. The generation of chromosomal deletions to provide extensive coverage and subdivision of the *Drosophila melanogaster* genome. Genome Biol. 13(3):R21. doi:10.1186/gb-2012-13-3-r21.

Coyle-Thompson CA, Banerjee U. 1993. The strawberry notch gene functions with Notch in common developmental pathways. Development. 119(2):377–395. doi:10.1242/dev.119.2.377.

Fernández-Espartero CH, Ramel D, Farago M, Malartre M, Luque CM, Limanovich S, Katzav S, Emery G, Martín-Bermudo MD. 2013. GTP exchange factor Vav regulates guided cell migration by coupling guidance receptor signalling to local Rac activation. J Cell Sci. 126(10):2285–2293. doi:10.1242/jcs.124438.

Furriols M, Bray S. 2001. A model Notch response element detects suppressor of Hairless-dependent molecular switch. Curr Biol. 11(1):60–64. doi:10.1016/S0960-9822(00)00044-0.

Ganguly A, Jiang J, Ip YT. 2005. *Drosophila* WntD is a target and an inhibitor of the Dorsal/Twist/Snail network in the gastrulating embryo. Development. 132(15):3419–3429. doi:10.1242/dev.01903.

Geisbrecht ER, Sawant K, Su Y, Liu ZC, Silver DL, Burtscher A, Wang X, Zhu AJ, McDonald JA. 2013. Genetic interaction screens identify a role for hedgehog signaling in *Drosophila* border cell migration. Dev Dyn. 242(5):414–431. doi:10.1002/dvdy.23926.

Gordon MD, Dionne MS, Schneider DS, Nusse R. 2005. WntD is a feedback inhibitor of Dorsal/NF-kappaB in *Drosophila* development and immunity. Nature. 437(7059):746–749. doi:10.1038/nature04073.

Grabbe C, Zervas CG, Hunter T, Brown NH, Palmer RH. 2004. Focal adhesion kinase is not required for integrin function or viability in *Drosophila*. Development. 131(23):5795–5805. doi:10.1242/dev.01462.

Hiremath C, Gao L, Geshow K, Patterson Q, Barlow H, Cleaver O, Marciano DK. 2023. Rap1 regulates lumen continuity via Afadin in renal epithelia. Dev Biol. 501:20–27. doi:10.1016/j.ydbio.2023.05.003.

Hu Y, Roesel C, Flockhart I, Perkins L, Perrimon N, Mohr SE. 2013. UP-TORR: online tool for accurate and up-to-date annotation of RNAi reagents. Genetics. 195(1):37–45. doi:10.1534/genetics.113.151340.

Huang H-C, Klein PS. 2004. The Frizzled family: receptors for multiple signal transduction pathways. Genome Biol. 5(7):234. doi:10.1186/gb-2004-5-7-234.

Hurd TR, Leblanc MG, Jones LN, DeGennaro M, Lehmann R. 2013. Genetic modifier screens to identify components of a redox-regulated cell adhesion and migration pathway. Methods Enzymol. 528:197–215. doi:10.1016/B978-0-12-405881-1.00012-4.

Jaśkiewicz A, Pająk B, Orzechowski A. 2018. The many faces of Rap1 GTPase. Int J Mol Sci. 19(10):E2848. doi:10.3390/ijms19102848.

Kim YS, Fan R, Lith SC, Dicke A-K, Drexler HCA, Kremer L, Kuempel-Rink N, Hekking L, Stehling M, Bedzhov I. 2022. Rap1 controls epiblast morphogenesis in sync with the pluripotency states transition. Dev Cell. 57(16):1937–1956.e8. doi:10.1016/j.devcel.2022.07.011.

Kim TY, Siesser PF, Rossman KL, Goldfarb D, Mackinnon K, Yan F, Yi X, MacCoss MJ, Moon RT, Der CJ, *et al.* 2015. Substrate trapping proteomics reveals targets of the βTrCP2/FBXW11 ubiquitin ligase. Mol Cell Biol. 35(1):167–181. doi:10.1128/MCB.00857-14.

Komander D, Clague MJ, Urbé S. 2009. Breaking the chains: structure and function of the deubiquitinases. Nat Rev Mol Cell Biol. 10(8):550–563. doi:10.1038/nrm2731.

Konstantinopoulos PA, Karamouzis MV, Papavassiliou AG. 2007. Post-translational modifications and regulation of the RAS superfamily of GTPases as anticancer targets. Nat Rev Drug Discov. 6(7):541–555. doi:10.1038/nrd2221.

Kotian N, Troike KM, Curran KN, Lathia JD, McDonald JA. 2022. A *Drosophila* RNAi screen reveals conserved glioblastoma-related adhesion genes that regulate collective cell migration. G3 (Bethesda). 12(1):jkab356. doi:10.1093/g3journal/jkab356.

Lei Z, Wang J, Zhang L, Liu CH. 2021. Ubiquitination-dependent regulation of small GTPases in membrane trafficking: from cell biology to human diseases. Front Cell Dev Biol. 9:688352. doi:10.3389/fcell.2021.688352.

Li H, Janssens J, De Waegeneer M, Kolluru SS, Davie K, Gardeux V, Saelens W, David FPA, Brbić M, Spanier K, *et al.* 2022. Fly cell atlas: a single-nucleus transcriptomic atlas of the adult fruit fly. Science. 375(6584):eabk2432. doi:10.1126/science.abk2432.

Llense F, Martín-Blanco E. 2008. JNK signaling controls border cell cluster integrity and collective cell migration. Curr Biol. 18(7):538–544. doi:10.1016/j.cub.2008.03.029.

Majumdar A, Nagaraj R, Banerjee U. 1997. Strawberry notch encodes a conserved nuclear protein that functions downstream of Notch and regulates gene expression along the developing wing margin of *Drosophila*. Genes Dev. 11(10):1341–1353. doi:10.1101/gad.11.10.1341.

Manseau L, Baradaran A, Brower D, Budhu A, Elefant F, Phan H, Philp AV, Yang M, Glover D, Kaiser K, *et al.* 1997. GAL4 enhancer traps expressed in the embryo, larval brain, imaginal discs, and ovary of *Drosophila*. Dev Dyn. 209(3):310–322. doi:10.1002/(SICI)1097-0177(199707)209:3%3C310::AID-AJA6%3E3.0.CO;2-L.

McDonald JA, Pinheiro EM, Montell DJ. 2003. PVF1, a PDGF/VEGF homolog, is sufficient to guide border cells and interacts genetically with Taiman. Development. 130(15):3469–3478. doi:10.1242/dev.00574.

McElwain MA, Ko DC, Gordon MD, Fyrst H, Saba JD, Nusse R. 2011. A suppressor/enhancer screen in *Drosophila* reveals a role for Wnt-mediated lipid metabolism in primordial germ cell migration. PLoS One. 6(11):e26993. doi:10.1371/journal.pone.0026993.

Messer CL, McDonald JA. 2023. Rap1 promotes epithelial integrity and cell viability in a growing tissue. Dev Biol. 501:1–19. doi:10.1016/j.ydbio.2023.05.006.

Miao G, Guo L, Montell DJ. 2022. Border cell polarity and collective migration require the spliceosome component Cactin. J Cell Biol. 221(7):e202202146. doi:10.1083/jcb.202202146.

Montell DJ, Yoon WH, Starz-Gaiano M. 2012. Group choreography: mechanisms orchestrating the collective movement of border cells. Nat Rev Mol Cell Biol. 13(10):631–645. doi:10.1038/nrm3433.

Niewiadomska P, Godt D, Tepass U. 1999. DE-cadherin is required for intercellular motility during *Drosophila* oogenesis. J Cell Biol. 144(3):533–547. doi:10.1083/jcb.144.3.533.

Öztürk-Çolak A, Marygold SJ, Antonazzo G, Attrill H, Goutte-Gattat D, Jenkins VK, Matthews BB, Millburn G, Dos Santos, Tabone CJ. 2024. FlyBase: updates to the Drosophila genes and genomes database. Genetics. 227(1). doi:10.1093/genetics/iyad211.

Patch K, Stewart SR, Welch A, Ward RE. 2009. A second-site noncomplementation screen for modifiers of Rho1 signaling during imaginal disc morphogenesis in *Drosophila*. PLoS One. 4(10):e7574. doi:10.1371/journal.pone.0007574.

Perez-Vale KZ, Yow KD, Gurley NJ, Greene M, Peifer M. 2023. Rap1 regulates apical contractility to allow embryonic morphogenesis without tissue disruption and acts in part via Canoe-independent mechanisms. Mol Biol Cell. 34(1):ar7. doi:10.1091/mbc.E22-05-0176.

Plutoni C, Keil S, Zeledon C, Delsin LEA, Decelle B, Roux PP, Carréno S, Emery G. 2019. Misshapen coordinates protrusion restriction and actomyosin contractility during collective cell migration. Nat Commun. 10(1):3940. doi:10.1038/s41467-019-11963-7.

Raaijmakers JH, Bos JL. 2009. Specificity in Ras and Rap signaling. J Biol Chem. 284(17):10995–10999. doi:10.1074/jbc.R800061200.

Rahimi N, Averbukh I, Haskel-Ittah M, Degani N, Schejter ED, Barkai N, Shilo B-Z. 2016. A WntD-dependent integral feedback loop attenuates variability in *Drosophila* toll signaling. Dev Cell. 36(4):401–414. doi:10.1016/j.devcel.2016.01.023.

Ramel D, Wang X, Laflamme C, Montell DJ, Emery G. 2013. Rab11 regulates cell-cell communication during collective cell movements. Nat Cell Biol. 15(3):317–324. doi:10.1038/ncb2681.

Roberto GM, Emery G. 2022. Directing with restraint: mechanisms of protrusion restriction in collective cell migrations. Sem Cell Dev Biol. 129:75–81. doi:10.1016/j.semcdb.2022.03.037.

Rothenberg KE, Chen Y, McDonald JA, Fernandez-Gonzalez R. 2023. Rap1 coordinates cell-cell adhesion and cytoskeletal reorganization to drive collective cell migration *in vivo*. Curr Biol. 33(13):2587–2601.e5. doi:10.1016/j.cub.2023.05.009.

Saadin A, Starz-Gaiano M. 2016. Circuitous genetic regulation governs a straightforward cell migration. Trends Genet. 32(10):660–673. doi:10.1016/j.tig.2016.08.001.

Sawant K, Chen Y, Kotian N, Preuss KM, McDonald JA. 2018. Rap1 GTPase promotes coordinated collective cell migration in vivo. Mol Biol Cell. 29(22):2656–2673. doi:10.1091/mbc.E17-12-0752.

Scarpa E, Mayor R. 2016. Collective cell migration in development. J Cell Biol. 212(2):143–155. doi:10.1083/jcb.201508047.

Schindelin J, Arganda-Carreras I, Frise E, Kaynig V, Longair M, Pietzsch T, Preibisch S, Rueden C, Saalfeld S, Schmid B, *et al.* 2012. Fiji: an open-source platform for biological-image analysis. Nat Methods. 9(7):676–682. doi:10.1038/nmeth.2019.

Schober M, Rebay I, Perrimon N. 2005. Function of the ETS transcription factor Yan in border cell migration. Development. 132(15):3493–3504. doi:10.1242/dev.01911.

Su W, Wynne J, Pinheiro EM, Strazza M, Mor A, Montenont E, Berger J, Paul DS, Bergmeier W, Gertler FB, *et al.* 2015. Rap1 and its effector RIAM are required for lymphocyte trafficking. Blood. 126(25):2695–2703. doi:10.1182/blood-2015-05-644104.

Sun H, Lagarrigue F, Ginsberg MH. 2022. The connection between Rap1 and Talin1 in the activation of integrins in blood cells. Front Cell Dev Biol. 10:908622. doi:10.3389/fcell.2022.908622.

Tsuda L, Nagaraj R, Zipursky SL, Banerjee U. 2002. An EGFR/Ebi/Sno pathway promotes delta expression by inactivating Su(H)/SMRTER repression during inductive notch signaling. Cell. 110(5):625–637. doi:10.1016/S0092-8674(02)00875-9.

Ueda Y, Higasa K, Kamioka Y, Kondo N, Horitani S, Ikeda Y, Bergmeier W, Fukui Y, Kinashi T. 2023. Rap1 organizes lymphocyte front-back polarity via RhoA signaling and talin1. iScience. 26(8):107292. doi:10.1016/j.isci.2023.107292.

Volovetz J, Berezovsky AD, Alban T, Chen Y, Lauko A, Aranjuez GF, Burtscher A, Shibuya K, Silver DJ, Peterson J, *et al.* 2020. Identifying conserved molecular targets required for cell migration of glioblastoma cancer stem cells. Cell Death Dis. 11(2):152. doi:10.1038/s41419-020-2342-2.

Walther RF, Burki M, Pinal N, Rogerson C, Pichaud F. 2018. Rap1, Canoe and Mbt cooperate with Bazooka to promote zonula adherens assembly in the fly photoreceptor. J Cell Sci. 131(6):jcs207779. doi:10.1242/jcs.207779.

Wang X, Adam JC, Montell D. 2007. Spatially localized Kuzbanian required for specific activation of Notch during border cell migration. Dev Biol. 301(2):532–540. doi:10.1016/j.ydbio.2006.08.031.

Wang X, He L, Wu YI, Hahn KM, Montell DJ. 2010. Light-mediated activation reveals a key role for Rac in collective guidance of cell movement in vivo. Nat Cell Biol. 12(6):591–597. doi:10.1038/ncb2061.

Wang Y-C, Khan Z, Wieschaus EF. 2013. Distinct Rap1 activity states control the extent of epithelial invagination via α-catenin. Dev Cell. 25(3):299–309. doi:10.1016/j.devcel.2013.04.002.

Ward RE, Evans J, Thummel CS. 2003. Genetic modifier screens in *Drosophila* demonstrate a role for Rho1 signaling in ecdysone-triggered imaginal disc morphogenesis. Genetics. 165(3):1397–1415. doi:10.1093/genetics/165.3.1397.

Wu C, Nusse R. 2002. Ligand receptor interactions in the Wnt signaling pathway in *Drosophila*. J Biol Chem. 277(44):41762–41769. doi:10.1074/jbc.M207850200.

Zegers MM, Friedl P. 2014. Rho GTPases in collective cell migration. Small GTPases. 5(3):e28997. doi:10.4161/sgtp.28997.

Zhang Y-L, Wang R-C, Cheng K, Ring BZ, Su L. 2017. Roles of Rap1 signaling in tumor cell migration and invasion. Cancer Biol Med. 14(1):90–99. doi:10.20892/j.issn.2095-3941.2016.0086.

Editor: D. Bergstralh